# Prussian blue modified iron oxide magnetic nanoparticles and their high peroxidase-like activity†

Xiao-Qing Zhang,[a] Shang-Wenyan Gong,[a] Yu Zhang,*[a] Ting Yang,[b] Chun-Yu Wang[b] and Ning Gu*[a]

*Received 27th January 2010, Accepted 25th March 2010*
*First published as an Advance Article on the web 14th May 2010*
**DOI: 10.1039/c0jm00174k**

Prussian blue (PB) modified $\gamma$-$Fe_2O_3$ magnetic nanoparticles (MNPs) featuring varying PB proportions were synthesized and characterized by TEM, FTIR, UV-vis, EDS, XRD and XPS. The magnetic properties and peroxidase-like catalytic activity of the synthesized nanoparticles were investigated. With increasing PB content, the magnetism could still maintain a high level. Peroxidase-like activity was enhanced as the PB proportion increased. Catalysis was found to follow Michaelis–Menten kinetics. The calculated kinetic parameters exhibited strong affinity with substrates and high catalytic activity, which are three orders of magnitudes larger than that for magnetite nanoparticles of similar size. Based on the high activity, an enzyme immunoassay model was established: staphylococcal protein A (SPA) was conjugated onto the surface of the nanoparticles to construct a new nanoprobe which was employed to detect IgG immobilized to 96-well plates. The results presented a linear absorbance enhancement with concentration of IgG, suggesting that PBMNPs serve as an inexpensive horseradish peroxidase (HRP) mimic enzyme with potential applications in bio-detection.

## Introduction

Magnetic iron oxide nanoparticles (NPs) have showed attractive prospects mainly in biomedical applications including protein immobilization and separation,[1,2] magnetic targeting and drug delivery,[3–6] cancer hyperthermia,[7,8] magnetic resonance imaging (MRI),[9–14] and so on. Recently, it was also reported that $Fe_3O_4$ NPs could possess intrinsic peroxidase-like activity.[15,16] This surprising finding makes magnetic $Fe_3O_4$ NPs powerful analytic tools to simultaneously realize capture, separation and detection. The peroxidase-like activity originates mainly from ferrous ions at the surface of NPs. The mechanism may follow the Fenton reaction.[15] The reaction can be written as (1) and (2), where $k_1$ and $k_2$ are reaction rate constants.

$$Fe^{2+} + H_2O_2 \rightarrow Fe^{3+} + {}^{\bullet}OH + OH^-;\ k_1 = 76\ L\ mol^{-1}\ s^{-1} \quad (1)$$

$$Fe^{3+} + H_2O_2 \rightarrow Fe^{2+} + {}^{\bullet}OOH + H^+;\ k_2 = 0.002\ L\ mol^{-1}\ s^{-1} \quad (2)$$

Step (2) has a low rate constant and is thus a rate-limited reaction process. The formed hydroxyl radical ($^{\bullet}OH$) plays an important role in oxidation of enzyme substrates, such as 3,3′,5,5′-tetramethylbenzidine (TMB), to lead to a color reaction.

$Fe_3O_4$ NPs are characterized by good compatibility, simple preparation, low cost, and mass production. As a result, $Fe_3O_4$ NPs could have a wide range of potential applications in chemical catalysis and biomedicine. However, magnetite ($Fe_3O_4$) is not very stable and is sensitive to oxidation, resulting in changes of the both magnetic properties and catalytic activity. Compared with $Fe_3O_4$ NPs, $\gamma$-$Fe_2O_3$ NPs are more stable with similar magnetism. Unfortunately, the peroxidase-like activity of $\gamma$-$Fe_2O_3$ NPs was demonstrated to be extremely weak in our pre-experiment due to the lack of ferrous ions at nanoparticle surfaces as indicated in eqn (1) and (2). Therefore, modification of $\gamma$-$Fe_2O_3$ NPs is needed, which can not only preserve its strong superparamagnetism but more importantly can improve catalytic activity. As a candidate for a surface modification agent, Prussian blue, $Fe^{III}_4[Fe^{II}(CN)_6]_3$, could provide the ferrous ions contributing to the catalytic reaction, and it has attracted much interest by many researchers.[17,18] Moreover, Prussian blue has exhibited excellent electrochemical behavior that can accelerate the electron transfer[19] and good catalytic property that could catalyze the reduction of hydrogen peroxidase.[20] Currently, it was reported that catalytic activity of NPs could be improved by optimizing their affinity toward substrates which could be enhanced by increasing electrostatic interaction between substrates and the nanoparticle surfaces.[21] TMB carries two amine groups with positive charge, likely yielding stronger affinity towards negatively charged nanoparticle surfaces. Hence, the modified $\gamma$-$Fe_2O_3$ should be of negative charge and the employed $[Fe(CN)_6]^{4-}$ might provide the source of negative charge at appropriate pH values.

We envisaged that when modified with PB, based on the excellent electrochemical behavior and catalytic property of PB as well as on the high stability and superparamagnetism of $\gamma$-$Fe_2O_3$, the resultant nanocomposites might show both superparamagnetism and peroxidase-like activity. In this study, we present a simple approach to synthesize $\gamma$-$Fe_2O_3$ nanoparticles modified by PB at different levels. The influence of the level of PB

[a]*Jiangsu key Laboratory for Biomaterials and Devices, State Key Laboratory of Bioelectronics, School of Biological Science and Medical Engineering, Southeast University, Nanjing, P.R. China*
[b]*School of Chemistry and Chemical Engineering, Southeast University, Nanjing, P.R. China. E-mail: zhangyu@seu.edu.cn; guning@seu.edu.cn; Fax: +86-(0)25-83272496; Tel: +86-(0)25-83272496*

† Electronic supplementary information (ESI) available: (1) Tables for establishment of immunoassay and element ratio of iron and nitrogen (EDS results); (2) UV-vis spectra of PBMNPs before and after the color reaction. See DOI: 10.1039/c0jm00174k

 

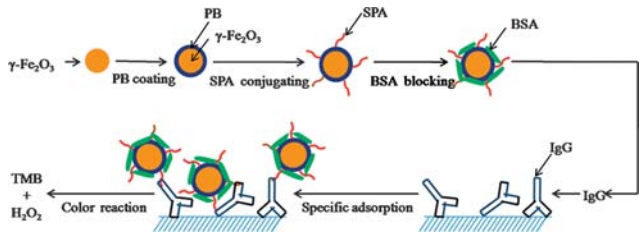


**Fig. 1** Schematic illustration of preparation of PBMNPs and immunoassays based on PBMNPs conjugated with SPA.

on the magnetism and peroxidase-like activity is investigated. Based on the high catalytic activity, the PBMNPs were further conjugated with staphylococcal protein A (SPA), to confirm its potential application in enzyme immunoassays. The total synthesis procedure of this study is as illustrated as Fig. 1.

## Experimental

### Chemicals and reagents

All chemicals used in this work were of analytical reagent grade. Deionized water was used throughout the study. Ferric chloride ($FeCl_3 \cdot 6H_2O$), ferrous sulfate ($FeSO_4 \cdot 7H_2O$), hydrochloric acid, hydrogen peroxide (30%), dimethyl sulfoxide (DMSO), 3,3′,5,5′-tetramethyibenzidine (TMB), potassium ferrocyanide ($K_4[Fe(CN)_6] \cdot 3H_2O$), anhydrous sodium acetate and acetic acid were purchased from Sinopharm Chemical Reagent Co. Ltd. Tetramethylammonium hydroxide, sodium dihydrogenphosphate, sodium hydrogencarbonate, anhydrous sodium carbonate, potassium chloride, sodium chloride, potassium dihydrogenphosphate and hydroxylammonium chloride were reagents from Shanghai Lingfeng Chemical Reagent Co. Ltd. Tween-20 and bovine serum albumin (BSA) were obtained from Sunshine. IgG, staphylococcal protein A (SPA) and bovine calf serum were purchased from Nanjing Booker Bio-Technology Co., Ltd.

### Preparation and characterization of pure and Prussian blue modified $\gamma$-$Fe_2O_3$ nanoparticles

The $\gamma$-$Fe_2O_3$ NPs were first prepared according to our previous work.[22] The particle concentration was then diluted to 0.1 mg $mL^{-1}$ and pH was adjusted to 2.0 with hydrochloric acid. The PBMNPs were prepared by an improved method[16] using the as-synthesized $\gamma$-$Fe_2O_3$ NPs as seeds under stirring, followed by adding dropwise varying amounts of an aqueous solution of 10 mg $mL^{-1}$ $K_4[Fe(CN)_6] \cdot 3H_2O$ with different volumes. The resultant mixture was continuously stirred for 1 h and the obtained composites were collected and washed three times by magnetic decantation. In this work, different amounts of $K_4[Fe(CN)_6] \cdot 3H_2O$ (1, 1.5, 2.5 mg) were selected to vary the PB content. The resultant PB modified $\gamma$-$Fe_2O_3$ magnetic nanoparticles are denoted as PBMNPs1, PBMNPs2 and PBMNPs3, respectively.

The particle size and morphology of the NPs obtained above were characterized by transmission electronic microscopy (TEM, JEOL JEM-2100). Fourier transform infrared spectroscopy (FTIR) analysis was performed using an infrared spectrometer (Nicolet AVATAR 360 FTIR). Ultraviolet–visible (UV-vis) absorption spectra were measured on an UV-VIS-NIR spectrophotometer (Shimadzu UV-3600, Japan). The structure and composition were detected by an X'TRA X-ray diffractometer ($\lambda = 1.54056$ Å) and X-ray photoelectron spectroscopy (XPS, Thermo ESCALAB 250), respectively. Energy dispersive spectrometer (EDS) was used to determine the element ratio of iron and nitrogen. Magnetic measurements were carried out with a Lakeshore 7407 vibrating sample magnetometer (VSM).

### Steady-state kinetic analysis

The steady-state kinetic assays were carried out at room temperature in a reaction system with 5 μL of $3.09 \times 10^{-10}$ M (in terms of nanoparticle molar concentration) PBMNPs3 in 1 mL of reaction buffer (0.1 M NaAc, pH = 4.6) in the presence of $H_2O_2$ and TMB. The kinetic analysis of PBMNPs3 with TMB as the substrate was performed by adding 64μL 30% $H_2O_2$ and different amounts (0, 1, 2, 4, 8, 12, 16, 20, 24μL) of TMB solution (10 mg $mL^{-1}$, dissolved in DMSO). The kinetic analysis of PBMNPs3 with $H_2O_2$ as the substrate was performed by adding 20 μL TMB and different amounts (0, 4, 8, 12, 16, 32, 64, 96 μL) of 30% $H_2O_2$ solution. All the reactions were monitored in timescan mode at 650 nm using the UV-VIS-NIR spectrophotometer. Catalytic parameters were determined by fitting the absorbance data to the Michaelis–Menten equation (3).

$$v = \frac{v_{max}[S]}{K_m + [S]} \quad (3)$$

The Michaelis–Menten equation describes the relationship between the rates of substrate conversion by an enzyme and the concentration of the substrate. In this equation, $v$ is the rate of conversion, $v_{max}$ is the maximum rate of conversion, [S] is the substrate concentration, and $K_m$ is the Michaelis constant. The Michaelis constant is equivalent to the substrate concentration at which the rate of conversion is half of $v_{max}$ and $K_m$ approximates the affinity of the enzyme for the substrate.

### Preparation of PBMNPs–SPA bioconjugates

In this study, both staphylococcal protein A (SPA) conjugating and BSA blocking were performed based on the electrostatic adsorption method, which is a common strategy used to graft protein onto the iron oxide nanoparticle surface.[23] SPA (100 μg) was dissolved in deionized water after which an equal amount of PBMNPs3 was added and the mixture was shaken at 37 °C for 1 h. Then the SPA conjugated PBMNPs3 was characterized by FTIR to confirm the successful conjugation. The blocking reaction was started by adding 5% BSA solution with continually shaking at 37 °C for 1 h. The resultant solution was stored at 4 °C for 12 h after which it was centrifuged at 10000 rpm for 30 min. The precipitation was resuspended in 1% BSA solution for further blocking and finally stored at 4 °C for use.

### IgG immunoassay

The suitability of the synthesized PBMNPs–SPA conjugates in bioaffinity assays was studied by performing an enzyme immunoassay for IgG. The immunoassay was carried out by incubating 100μL of various concentrations of IgG (1, 1.5, 2 and 2.5 μg $mL^{-1}$) suspended in carbonate buffer (CB, pH = 9.0) at 37 °C for 1 h. After that, the wells were washed three times by

PBS-T (pH = 7.4, Tween-20 = 0.05 mass%) and 200 μL of 10% bovine calf serum (BCS) was added into wells at 37 °C for 1 h to block the possible remaining binding sites. The wells were washed again by PBS-T and the SPA conjugated nanoparticles were added into 100 μL wells for 1 h. After washing the wells three times, the substrate solution was added to the wells for 30 min and the absorbance was measured by a microplate reader (BIO-RAD model 680). In this study, two blank controls and a negative control were set. One of the blank controls was that the wells were untreated and the other blank control was treated at the last PBMNPs-SPA incubating step with 1% BSA solution (no PBMNPs-SPA). The negative control was treated at the first step with no IgG incubation and the same volume of carbonate buffer. All the settings of control groups and procedure to treat the wells are given in Table S1 in the ESI†.

## Results and discussion

### Formation mechanism of the PB modified γ-$Fe_2O_3$ nanoparticles

Since there is a large surface/volume ratio, high surface activity, and a high amount of dangling bonds on the NP surfaces, the atoms on the surface are apt to adsorb ions. In dilute acidic solution, the surface charge of γ-$Fe_2O_3$ NPs is positive (zeta potential was measured to be about 30 mV), and $[Fe(CN)_6]^{4-}$ can be attracted on the surface of γ-$Fe_2O_3$ NPs for the electrostatic interactions; on the other hand, $CN^-$ can stably complex to ferric ions at the surface of MNPs, resulting also in $[Fe(CN)_6]^{4-}$ adsorption. Both of the two factors promote the adsorption of $[Fe(CN)_6]^{4-}$, resulting in the formation of a PB coating. Further coordination with $Fe^{3+}$ which was released from γ-$Fe_2O_3$ NPs in the reaction system (pH = 2) will generate more PB coating on the surface of the NPs. The dissolved $Fe^{3+}$ in the reaction mixture was confirmed by using a well known spot test.[24] This method is based on the fact that $Fe^{III}$ can be reduced to $Fe^{II}$ by hydroxylamine hydrochloride and $Fe^{II}$ salts in acidic solutions react with α,α-phenanthroline to give a soluble, dark red complex. The structure and composition of the nanocomposites were further confirmed by FTIR spectra, UV-Vis spectra, XRD, EDS and XPS analysis as below.

### Structural and compositional characterization of pure and PB-modified γ-$Fe_2O_3$ nanoparticles

TEM images (Fig. 2) shows the particle size and corresponding distribution of the as-synthesized samples. Before modification, the average size of γ-$Fe_2O_3$ NPs is about 9.5 nm. After modification with PB, the particles tend to be slightly larger and the size is approximately 9.8, 10 and 10.5 nm for PBMNPs1, PBMNPs2 and PBMNPs3, respectively. This may be due to the modified PB on the surface of γ-$Fe_2O_3$ NPs but the size increases a little with increasing PB proportion due likely also to the surface decomposition of γ-$Fe_2O_3$ NPs in the reaction process. The obtained PBMNPs could be stably dispersed in aqueous solution. The average hydrodynamic diameter of PBMNPs was in the range of 120 and 160 nm as characterized by dynamic light scattering (DLS). A typical curve is presented in the ESI† (Fig. S1).

The FTIR absorption spectra (Fig. 3) give a comparison between PB-modified and pure γ-$Fe_2O_3$ NPs. The spectrum of the PBMNPs exhibited a peak at 2110 $cm^{-1}$ attributed to the CN

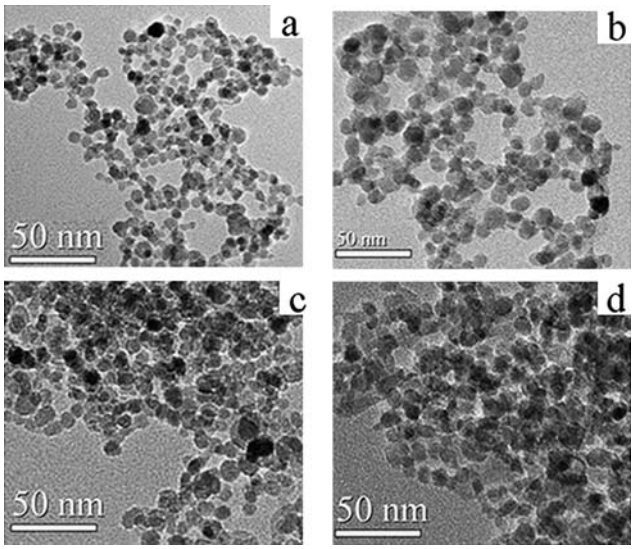


**Fig. 2** TEM photographs of (a) γ-$Fe_2O_3$ NPs, (b) PBMNPs1, (c) PBMNPs2 and (d) PBMNPs3.

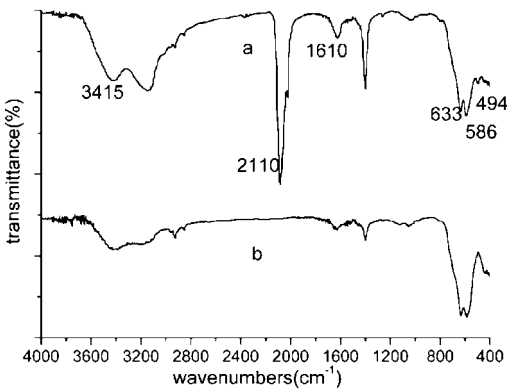


**Fig. 3** FTIR spectra of (a) γ-$Fe_2O_3$ NPs and (b) PBMNPs.

stretching in the formed $[Fe^{II}–CN–Fe^{III}]$ structure,[25] and an absorption band at 494 $cm^{-1}$ is also due to the formation of $[Fe^{II}–CN–Fe^{III}]$,[26] which indicates the presence of PB. The bands near 468 and 547 $cm^{-1}$ were characteristic absorptions of Fe–O bond for bulk γ-$Fe_2O_3$.[27] However, in Fig. 3, the bands shift to higher wavenumbers of 586 and 633 $cm^{-1}$. A basic effect of the finite size of NPs is the breaking of a large number of bonds for surface atoms, resulting in the rearrangement of dissociative electrons on the particle surface. Hence, when particles are reduced to nanoscale dimensions, the absorption bands of FTIR spectra shift to higher wavenumbers.[28] In addition, the absorption bands near 3415 and 1610 $cm^{-1}$ refer to the O–H stretching mode and H–O–H bending mode, respectively, indicating the presence of interstitial water in the samples.[29]

UV-vis absorption spectra (Fig. 4) present the typical curves of γ-$Fe_2O_3$ and PBMNPs with different proportion of PB. In the case of unmodified maghemite particles, no obvious absorption peak could be observed, while for PB modified γ-$Fe_2O_3$, the mixed-valence charge-transfer band at 700 nm of the polymeric $[Fe^{II}–CN–Fe^{III}]$ sequence can be observed, which is in accordance with the literature previously reported.[30,31] Further, it is clear that

 

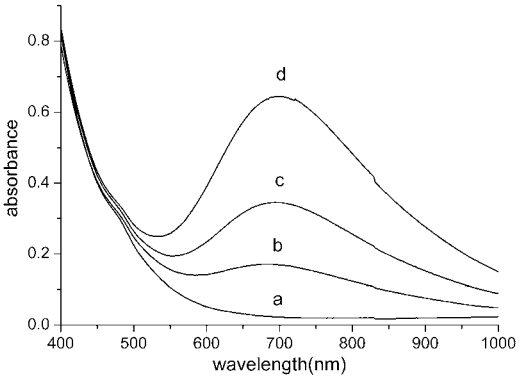


**Fig. 4** UV-vis absorption spectra of (a) $\gamma$-$Fe_2O_3$ NPs, (b) PBMNPs1, (c) PBMNPs2 and (d) PBMNPs3.

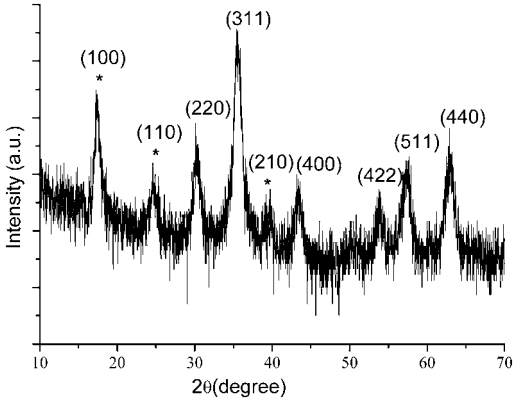


**Fig. 5** XRD pattern of PBMNPs3.

at the same nanoparticle molar concentration, the band at 700 nm for PBMNPs increases with the amount of coated PB on the nanoparticle surfaces. The elemental distribution for the iron and nitrogen in PBMNPs was tested by energy dispersive spectrometry (EDS) and the data (Table S2, ESI†) shows both the atom and weight ratios for nitrogen to iron increase when the PB proportion increases. The molar ratio of coated PB to core $\gamma$-$Fe_2O_3$ was calculated by EDS results, as 0.087, 0.179 and 0.240 for PBMNPs1, PBMNPs2 and PBMNPs3 respectively. The PB loading capacity was consistent with the UV-vis spectra indicating the fact that $\gamma$-$Fe_2O_3$ NPs were coated with PB.

The phase structure of the MNPs and PBMNPs were identified by XRD. From a typical XRD pattern (in Fig. 5) for PBMNPs3, we can see the characteristic peaks of (220), (311), (400), (422), (511) and (440) indicating the cubic spinel structure of $\gamma$-$Fe_2O_3$.[22] The peaks of (100), (110) and (210) are the characteristic peaks of PB,[32] suggesting that the coating layer indeed was of PB. XPS was used for evaluating the composition and element valence state of the pure and PB-modified $\gamma$-$Fe_2O_3$ NPs. Wide range (or survey XPS) spectra for pure and modified nanoparticles are shown in Fig. 6A. Comparison of the two curves reveals that curve b has a distinctive N (N 1s) peak (396 eV) and shows a relative increase of the C (C 1s, 284 eV) signal, indicating the existence of –CN groups. The detailed Fe 2p spectra of the products corresponding to the binding energies are depicted by Fig. 6B, which shows that the binding energies relating to Fe $2p_{3/2}$ and Fe $2p_{1/2}$ are about 710 and 725 eV, respectively. For $\gamma$-$Fe_2O_3$ NPs, it can be clearly seen that shakeup satellites occur in the 716–720 eV region (curve a in Fig. 6B), which is characteristic for $Fe^{3+}$ ions in $Fe_2O_3$.[33] After employment of PB (curve b in Fig. 6B), the shakeup satellites became weakened, implying the formation of a PB coating on the surface of $\gamma$-$Fe_2O_3$ NPs. A weak shoulder of the main Fe $2p_{3/2}$ peak at lower binding energies (708.4 eV) occurs for the PB-modified $\gamma$-$Fe_2O_3$ NPs (Fig. 6B(b)), indicating the existence of $Fe^{2+}$ ions in Prussian blue.[34] From these results, the structure of the PBMNPs is further confirmed and the ferrous ions actually exist with no oxidation to ferric ions in the nanocomposites. As described above, the catalytic activity is mainly due to ferrous ions.

## Magnetism

Magnetic measurement indicates superparamagnetic behavior at room temperature for all samples (Fig. 7), with no hysteresis and perfect Langevin behavior. The saturation magnetization value ($M_s$) for $\gamma$-$Fe_2O_3$ NPs is 47.52 emu $g^{-1}$ while $M_s$ for PBMNPs1, PBMNPs2 and PBMNPs3 are decreased to 44.13, 39.4 and 34.73 emu $g^{-1}$, respectively. The presence of weak magnetic PB on the surface of the modified nanoparticles leads to decrease of $M_s$ while partial dissolution of the magnetic $\gamma$-$Fe_2O_3$ cores in the synthetic process also results in a decrease of $M_s$. Although there is a small decrease, the nanocomposites still maintain a sufficient

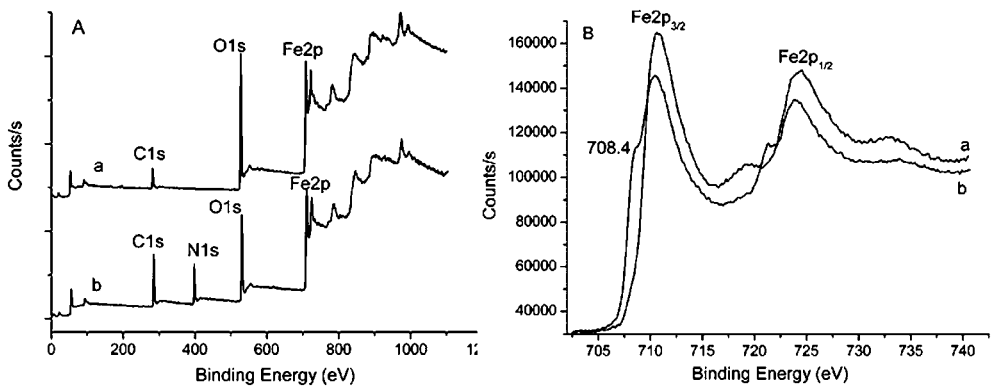


**Fig. 6** XPS (A) wide spectra and (B) Fe 2p core-level spectra for both (a) $\gamma$-$Fe_2O_3$ and (b) PB modified $\gamma$-$Fe_2O_3$ nanoparticles.

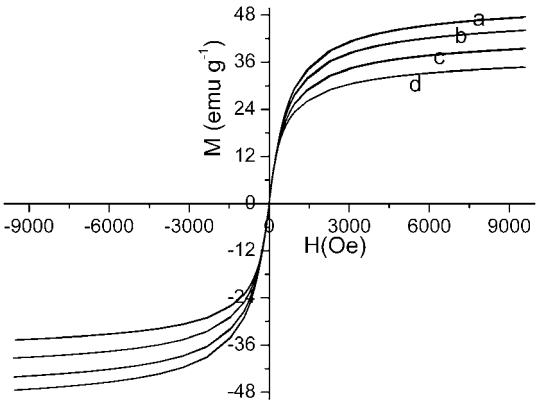


**Fig. 7** Hysteresis loops at room temperature of (a) γ-$Fe_2O_3$ NPs, (b) PBMNPs1, (c) PBMNPs2 and (d) PBMNPs3.

value of $M_s$ for magnetic application when modified with Prussian blue.

### Peroxidase-like activity

The peroxidase-like behavior of the synthesized NPs was examined using TMB as a chromogenic substrate. TMB has been proved to be a noncarcinogenic derivative[35] and can be oxidized to a blue reaction product with maximum absorbance at 370 and 650 nm in the presence of $H_2O_2$. [36] Fig. 8 shows the UV-vis absorption spectra of the γ-$Fe_2O_3$ and PBMNPs catalytic reaction systems upon reaction for 15 min. As shown in Fig. 8, two peaks are observed at 369 and 650 nm, indicating that TMB was oxidized. Fig. 9 presents the time course curves of the different reaction systems catalyzed by pure MNPs, PBMNPs1, PBMNPs2 and PBMNPs3 within 25 min. After the color reaction, PBMNPs3 were also examined by UV-vis spectroscopy and presented similar characteristic absorption peaks to that of unreacted PBMNPs3 (ESI†, Fig. S2), suggesting a relatively good stability of the PB coating in the reaction process. Since the intrinsic color of PB may contribute to the absorption of the color reaction a control was established by incubating an equal quantity of PBMNPs3 in the same buffer with no TMB and $H_2O_2$ for the same time (curve a in Fig. 9). It is obvious that the influence of PB color is negligible owing to the very low absorbance of the control group. At the same molar nanoparticle

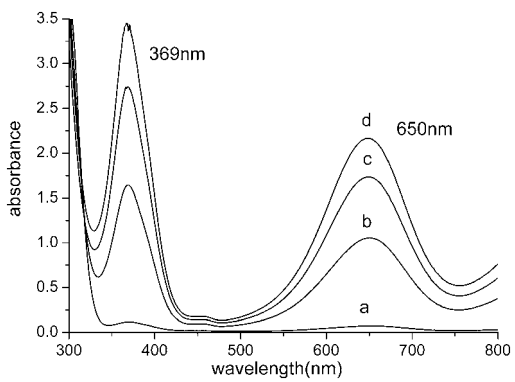


**Fig. 8** UV-vis absorption spectra of the TMB–$H_2O_2$ reaction system catalyzed by (a) γ-$Fe_2O_3$ NPs, (b) PBMNPs1, (c) PBMNPs2 and (d) PBMNPs3 for 15 min.

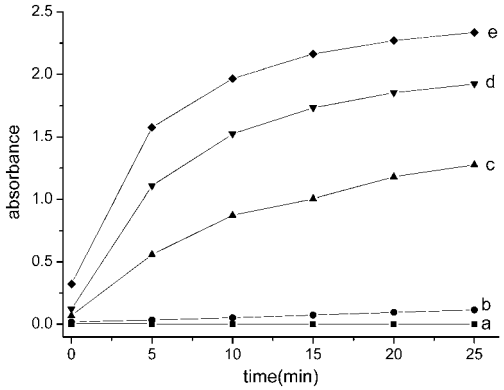


**Fig. 9** UV-vis absorption–time course curves of (a) a control for PBMNPs in the same buffer without TMB–$H_2O_2$ and reaction system catalyzed by (b) γ-$Fe_2O_3$ NPs, (c) PBMNPs1, (d) PBMNPs2 and (e) PBMNPs3.

concentration, MNPs can scarcely catalyze the reaction (as characterised by low absorbance) compared to the PBMNPs; when modified with PB, the absorbance reached much higher value. The PBMNPs showed different levels of activity towards TMB in the order PBMNPs3 > PBMNPs2 > PBMNPs1, that is, the higher the level of PB, and the higher the catalytic activity. This phenomenon may be due to the more PB providing more ferrous ions as catalysis centers to interact with substrates. Based on much higher catalytic activity, PBMNPs3 was applied in the kinetic analysis and immunoassays.

### Steady-state kinetics

The apparent steady-state kinetic parameters for the reaction were determined at room temperature and PBMNPs3 were employed as the catalytic agent. Absorbance data were back-calculated to concentration by the Beer–Lambert Law using a molar absorption coefficient of 39000 $M^{-1}cm^{-1}$ for TMB-derived[37] oxidation products. Apparent steady-state reaction rates at different concentrations of substrate were obtained by calculating the slopes of initial absorbance changes with time. The curves shown in Fig. 10 indicate that the reaction catalyzed by PBMNPs3 displayed Michaelis–Menten kinetics.

Data was fitted to the Michaelis–Menten equation (curves shown in Fig. 10) to obtain the catalytic parameters, as shown in Table 1. The $K_m$ value of PBMNPs3 with $H_2O_2$ as the substrate was significantly higher than that for HRP, consistent with the observation that a higher concentration of $H_2O_2$ was required to obtain maximal reaction velocity for PBMNPs3. The $K_m$ value of the PBMNPs3 with TMB as the substrate was a little lower than for HRP (Table 1), suggesting that the PBMNPs3 have a slightly higher affinity for TMB than HRP. At the same molar concentration, the $k_{cat}$ value of PBMNPS3 and HRP showed a similar level of activity. The $k_{cat}/K_m$ value of the PBMNPs3 and HRP with TMB as substrate appeared similar. The $k_{cat}/K_m$ value of the PBMNPs3 with $H_2O_2$ as substrate was significantly smaller than that for HRP, corresponding to the larger $K_m$ value for $H_2O_2$.

As a catalytic agent, compared with HRP, PBMNPs3 exhibits similar catalytic efficiency. There may be many ferrous ions at the surface of PBMNPs3, providing more active sites for catalysis while HRP has only one active site. Supposing that, the high

 

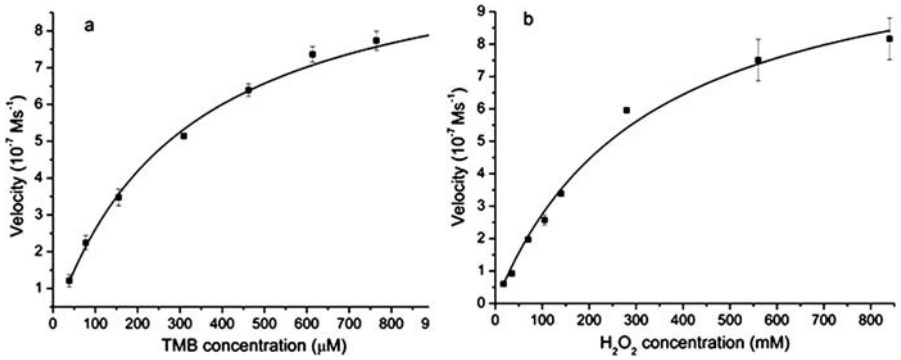


**Fig. 10** Kinetic analysis for PBMNPs3 with (a) TMB and (b) $H_2O_2$ as substrates, respectively. A steady-state catalysis rate was calculated from the initial slopes of absorbance *vs*. time curves.

**Table 1** Comparison of the kinetic parameters of PBMNPs3 and HRP[a]

| | [E]/M | Substrate | $K_m$/mM | $v_{max}$/M s$^{-1}$ | $k_{cat}$/s$^{-1}$ | ($k_{cat}/K_m$)/M$^{-1}$ s$^{-1}$ |
|---|---|---|---|---|---|---|
| PBMNPs3 | $3.09 \times 10^{-10}$ | TMB | 0.307 | $1.06 \times 10^{-6}$ | $3.43 \times 10^{3}$ | $1.1 \times 10^{7}$ |
| | | $H_2O_2$ | 323.6 | $1.17 \times 10^{-6}$ | $3.79 \times 10^{3}$ | $1.2 \times 10^{4}$ |
| HRP[15] | $2.5 \times 10^{-11}$ | TMB | 0.434 | $10.00 \times 10^{-8}$ | $4.00 \times 10^{3}$ | $9.2 \times 10^{6}$ |
| | | $H_2O_2$ | 3.7 | $8.71 \times 10^{-8}$ | $3.48 \times 10^{3}$ | $9.4 \times 10^{5}$ |

[a] [E] is nanoparticle and HRP concentration, $K_m$ is the Michaelis constant, $v_{max}$ is the maximal reaction velocity and $k_{cat}$ is the catalytic constant, where $k_{cat} = v_{max}/[E]$. Note that the $k_{cat}$ value shows the catalytic efficiency per nanoparticle.

catalytic efficiency can be attributed to the collective effect of ferrous ions. The collective effect may be a function of the nanoparticle size, that is, there are more ions at the larger nanoparticle surface than at the smaller ones. Therefore, it can be explained why the $k_{cat}$ value with TMB of Yan's[15] $Fe_3O_4$ MNPs is higher than that of our PBMNPs3. PBMNPs3 were about 10 nm while Yan's $Fe_3O_4$ MNPs were about 300 nm in size. Normalization processing was thus made for the $k_{cat}$ value according to surface area $S$. The value of $k_{cat}/S$ was 9.9 s$^{-1}$ nm$^{-2}$ for PBMNPs3, much greater than 0.11 s$^{-1}$ nm$^{-2}$ for Yan's $Fe_3O_4$ MNPs. An additional comparison with a similar size of $Fe_3O_4$ nanoparticles[21] was made to emphasize the role of PB coating in enhancement of peroxidase-like activity. Yang's group[21] studied the impact of six different coatings on the peroxidase activity of $Fe_3O_4$ NPs. The $k_{cat}$ value was in the range of 0.43–2.45 s$^{-1}$ by a rough calculation in terms of nanoparticle concentration, which was about three orders of magnitudes lower than our PB modified $\gamma$-$Fe_2O_3$ nanoparticles. In general, the high catalytic efficiency of PBMNPs3 may be due to (i) $Fe^{2+}$ ions in the PBMNPs3 playing a dominant role in the catalytic peroxidase-like activity, which is consistent with Yang's viewpoint of that $Fe^{2+}$ in the $Fe_3O_4$ MNPs contributes to the catalytic activity; (ii) the zeta potential of PBMNPs was measured to be at the range of −27 and −32 mV, which can enhance the affinity between the catalyst and the positively charged TMB substrate.

## IgG immunoassay

Fig. 11 shows the nanoparticle concentration dependency of the peroxidase-like activity. There is a linear absorbance increase with a correlation coefficient of 0.988 as a function of PBMNPs3 concentration, indicating that PBMNPs3 can be used as a mimic enzyme label in bioanalysis. The PBMNPs3-SPA conjugates were successfully prepared, as demonstrated by FTIR measurement (Fig. S3, ESI†). The PBMNPs-SPA nanoparticles were applied in the enzyme immunoassays to further confirm the potential application in bio-detection. As shown in Fig. 12, the control 1 displayed an absorption of about 0.1, which may be attributed to spontaneous oxidation of TMB in the presence of $H_2O_2$. Absorption for control 2 was a litter lower, due to the extra treatment leading to a possible change of refraction. The negative control exhibited a little higher absorption than controls 1 and 2, a possible reason may be that incubated PBMNPs-SPA nanoparticles could not be washed thoroughly and remained at the bottom or on the wall of the wells, resulting in inevitable catalytic reaction. From the results of the four positive groups, we can see that, the absorbance increases linearly with the concentration of IgG with a correlation coefficient of

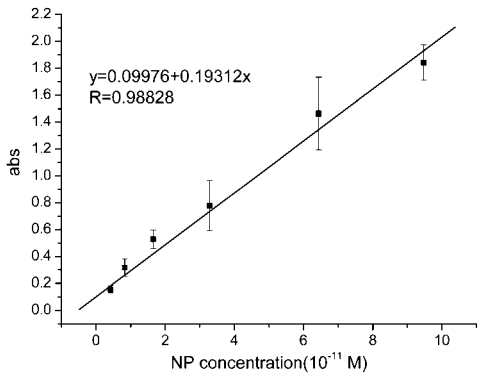


**Fig. 11** Concentration dependency of peroxidase-like activity for PBMNPs3.

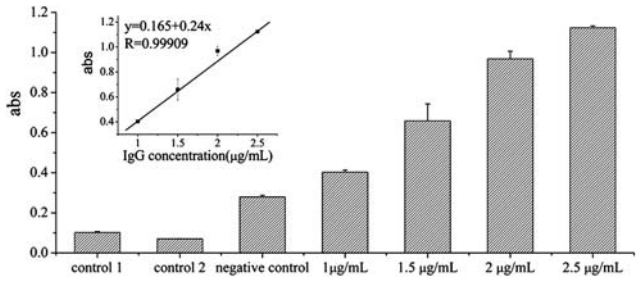


**Fig. 12** Immunoassays based on the peroxidase-like activity of PBMNPs3.

0.999 (Fig. 12, inset), suggesting that PBMNPs-SPA can retain peroxidase-like activity and specifically bind to IgG immobilized at well plates. The linear increase of the absorbance as a function of IgG concentration is of significance for biological detection.

## Conclusion

Prussian blue modified $\gamma$-$Fe_2O_3$ nanoparticles were prepared by a simple method and characterized by TEM, FTIR, UV-vis, EDS, XRD, XPS and VSM. The resultant nanocomposite not only retained strong superparamagnetism but also possessed intrinsic peroxidase-like activity. Peroxidase-like catalytic activity was enhanced as function of PB level. Catalysis by PBMNPs showed typical Michaelis–Menten kinetics, and exhibited high catalytic efficiency. As nanoparticle enzyme mimetics, Prussian blue modified $\gamma$-$Fe_2O_3$ nanoparticles display the highest $k_{cat}$ value to the best of our knowledge. An enzyme immunoassay was performed based on the catalytic activity; upon conjugation with SPA, PBMNPs could specifically combine with IgG immobilized in the wells. These studies show potential application of PBMNPs in bio-detection.

## Acknowledgements

This work is supported by the National Natural Science Foundation of China (No. 30870679,30970787) and the National Basic Research Program of China (Nos. 2006CB933206, 2006CB705606). The program for New Century Excellent Talents in University and the Chinese Ministry of Education are greatly appreciated.

## References

1 J. M. Perez, F. J. Simeone, A. Tsourkas, L. Josephson and R. Weissleder, *Nano Lett.*, 2004, **4**, 119.
2 B. M. Oscar, P. M. Maria, T. Pedro, R. C. Jesus, B. Pierre, S. Martin, X. Q. Zhao and V . V. Sabino, *Biomaterials*, 2005, **26**, 5695.
3 J. J. Cheng, B. A. Teply, S. Y. Jeong, C. H. Yim, D. Ho, I. Sherifi, S. Jon, O. C. Farokhzad, A. R. Khademhosseini and S. Langer, *Pharm. Res.*, 2006, **23**, 557.
4 Y. Yang, J. S. Jiang, B. Du, Z. F. Gan, M. Qian and P. Zhang, *J. Mater. Sci.: Mater. Med.*, 2009, **20**, 301.
5 M. L. Gou, Z. Y. Qian, H. Wang, Y. B. Tang, M. J. Huang, B. Kan, Y. J. Wen, M. Dai, X. Y. Li, C. Y. Gong and M. J. Tu, *J. Mater. Sci.: Mater. Med.*, 2008, **19**, 1033.
6 H. Tanaka, T. Sugita, Y. J. Yasunaga, S. J. Shimose, M. Deie, T. Kubo, T. Murakami and M. Ochi, *J. Biomed. Mater. Res., Part A*, 2005, **73a**, 255.
7 M. L. Matteucci, G. Anyarambhatla, G. Rosner, C. Azuma, P. E. Fisher, M. W. Dewhirst, D. Needham and D. E. Thrall, *Clin. Cancer Res.*, 2000, **6**, 3748.
8 I. J. Majoros, A. Myc, T. Thomas, C. B. Mehta and J. R. Baker, *Biomacromolecules*, 2006, **7**, 572.
9 M. Brähler, R. Georgieva, N. Buske, A. Muller, S. Muller, J. Pinkernelle, U. Teichgraber, A. Voigt and H. Banmler, *Nano Lett.*, 2006, **6**, 2505.
10 M. C. Denis, U. Mahmood, C. Benoist, D. Mathis and R. Weissleder, *Proc. Natl. Acad. Sci. U. S. A.*, 2004, **101**, 12634.
11 J. W. Bulte, *Methods Mol. Med.*, 2006, **124**, 419.
12 M. Modo, M. Hoehn and J. W. Bulte, *Mol. Cellular Magn. Reson. Imaging*, 2005, **4**, 143.
13 C. Burtea, S. Laurent, A. Roch, L. Vander Elst and R. N. Muller, *J. Inorg. Biochem.*, 2005, **99**(5), 1135.
14 S. Boutry, S. Laurent, L. Vander Elst and R. N. Muller, *Contrast Media Mol. Imaging*, 2006, **1**, 15.
15 L. Z. Gao, J. Zhuang, L. Nie, J. B. Zhang, Y. Zhang, N. Gu, T. H. Wang, J. Feng, D. L. Yang, S. Perrett and X. Y. Yan, *Nat. Nanotechnol.*, 2007, **2**, 577.
16 H. Wei and E. K. Wang, *Anal. Chem.*, 2008, **80**, 2250.
17 J. T. Culp, J. H. Park, D. Stratakis, M. W. Meisel and D. R. Talham, *J. Am. Chem. Soc.*, 2002, **124**, 10083.
18 G. D. Liang, J. T. Xu and X. S. Wang, *J. Am. Chem. Soc.*, 2009, **131**, 5378.
19 Y. Zhuo, P. X. Yuan, R. Yuan, Y. Q. Chai and C. L. Hong, *Biomaterials*, 2009, **30**, 2284.
20 E. Y. Sun, L. Josephson, K. A. Kelly and R. Weissleder, *Bioconjugate Chem.*, 2006, **17**, 109.
21 F. Q. Yu, Y. Z. Huang, A. J. Cole and V. C. Yang, *Biomaterials*, 2009, **30**, 4716.
22 Y. K. Sun, M. Ma, Y. Zhang and N. Gu, *Colloids Surf., A*, 2004, **245**, 15.
23 T. Suwa, S. Ozawa, M. Ueda, N. Ando and M. Kitajima, *Int. J. Cancer*, 1998, **75**, 626.
24 R. Abu-Much, U. Meridor, A. Frydman and A. Gedanken, *J. Phys. Chem. B*, 2006, **110**, 8194.
25 J. B. Ayers and W. H. Piggs, *J. Inorg. Nucl. Chem.*, 1971, **33**, 721.
26 R. E. Wilde, S. N. Ghosh and B. Marshall, *Inorg. Chem.*, 1970, **9**, 2512.
27 R. D. Waldron, *Phys. Rev.*, 1955, **99**, 1727.
28 G. Zhao, J. J. Feng, Q. L. Zhang, S. P. Li and H. Y. Chen, *Chem. Mater.*, 2005, **17**, 3154.
29 K. Itaya, I. Uchida and V. D. Neff, *Acc. Chem. Res.*, 1986, **19**, 162.
30 M. Pyrasch and B. Tieke, *Langmuir*, 2001, **17**, 7706.
31 W. Zhao, J. J. Xu, C. G. Shi and H. Y. Chen, *Langmuir*, 2005, **21**, 9630.
32 S. Q. Liu, J. J. Xu and H. Y. Chen, *Electrochem. Commun.*, 2002, **4**, 421.
33 (*a*) J. F. Anderson, M. Kuhn and U. Diebold, *J. Cryst. Growth*, 1997, **174**, 446; (*b*) W. Kim, K. Kawaguchi, N. Koshizaki, M. Sohma and T. Matsumoto, *J. Appl. Phys.*, 2003, **93**, 8032.
34 K. B. Yatsimirskii, V. V. Nemoshalenko, Y. P. Nazarenko, V. G. Aleshin, V. V. Zhilinskaya and N. A. Tomashevsky, *J. Electron Spectrosc. Relat. Phenom.*, 1977, **10**, 239.
35 S. Savard and P. D. Josephy, *Mutagenesis*, 1987, **2**, 97.
36 P. D. Josephygg, T. Elingg and R. P. Mason, *J. Biol. Chem.*, 1982, **257**, 3669.
37 E. I. Karaseva, Y. P. Losev and D. I. Metelitsa, *Russ. J. Bioorg. Chem.*, 2002, **28**, 128.

 